# Fast Small Offshore Target Detection Based on Object Region Characteristic[1)]

ZOU Yu-Lan WANG Guo-You ZHANG Lei

(*Institute for Pattern Recognition and Artificial Intelligence, State Education Commission Key Laboratory for Image Processing and Intelligent Control, Huazhong University of Science & Technology, Wuhan* 430074)
(E-mail: snow.zyl@163.com)

**Abstract** A fast object detection method based on object region dissimilarity and 1-D AGADM (one dimensional average gray absolute difference maximum) between object and background is proposed for real-time defection of small offshore targets. Then computational complexity, antinoise performance, the signal-to-noise ratio (SNR) gain between original images and their results as a function of SNR of original images and receiver operating characteristic (ROC) curve are analyzed and compared with those existing methods of small target detection such as two dimensional average gray absolute difference maximum (2-D AGADM), median contrast filter algorithm and multi-level filter algorithm. Experimental results and theoretical analysis have shown that the proposed method has faster speed and more adaptability to small object shape and also yields improved SNR performance.

**Key words** Small target detection, average gray absolute difference maximum, computational complexity, signal-to-noise ratio (SNR), ROC curve

## 1 Introduction

Because the features of multiscale small targets object such as shape, texture, moment, structure, motion continuity and fractals are undeterministic and distinctness, most of the existing methods[1∼3] based on shape, texture, and structure of the targets lose their validity. Even the fractal technique[4] also can not provide satisfactory detection performance. Therefore, we proposed a dissimilarity measure between object and its background to enhance the ratio of the signal to noise of small objects, and increase the detectable probability[5] under low false alarm probability. In order to adapt real time image processing applications to long-wave infrared offshore small-object images detection, a dissimilarity measurement of one-dimensional average gray absolute difference maximum (1-D AGADM), and their characteristic are discussed, then fast algorithm for multiscale small object detection in a nature scene with a spatially independent and stable Gaussian random field is derived and tested.

## 2 Theory of small target detection

The methods of small target detection can be classified as

1) Minimum false probability-based methods, which are feasible when the probability distribution of object and background can be known.

2) Constant false alarm probability-based methods, which are feasible when the probability distribution of a background can be known but the object distribution is undeterministic.

3) Constant detectable probability-based methods, which are valid when the probability distribution of an object can be known but the background distribution is undeterministic.

In order to improve the performance of small target detection, we propose an algorithm by using average gray absolute difference maximum map (AGADMM) to enhance an object while capable of reducing its background[6].

### 2.1 Definition of dissimilarity measure

As show in Fig. 1, set $\Theta$ and $\Omega$ denote the pixels in the internal window and pixels between internal window and external window, respectively. If the size of external window is slightly bigger than that of the object and internal window can be changed, then the AGADM can be defined as:

$$\Delta D_{\max} = \max_{\forall \Theta} \left\{ \Delta D | \Delta D = \left| \frac{1}{N_\Theta} \sum_{x \in \Theta} I_x - \frac{1}{N_\Omega} \sum_{y \in \Omega} I_y \right| \right\} \tag{1}$$

1) Supported by the National Defense Science Foundation of P. R. China (51401020201JW0521)
Received September 26, 2003; in revised form October 30, 2004

where $N_\Theta, N_\Omega$ denote the numbers of pixels in set $\Theta$ and $\Omega$, $I_x$ and $I_y$ denote the gray levels of pixel $x$ and $y$, respectively.

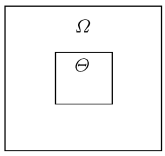


Fig. 1 Object and scene windows

It has been shown that AGADM has a low value if set $\Theta$ and $\Omega$ include only the pixels in a background, and reach the largest response when set $\Theta$ and $\Omega$ cover only the pixels of an object and background, respectively[6]. If the target shape is not square, then $\Theta$ includes the pixels of object $\Theta_o$ and partial background $\Theta_b$, that is,

$$\Delta D = \left|\frac{1}{N_\Theta}\sum_{x\in\Theta} I_x - \frac{1}{N_\Omega}\sum_{y\in\Omega} I_y\right| = \left|\frac{N_{\Theta_o}}{N_\Theta}\bar{I}_o + \frac{N_\Theta - N_{\Theta_o}}{N_\Theta}\bar{I}_{b\Theta} - \bar{I}_{b\Omega}\right| =$$
$$\left|\frac{N_{\Theta_o}}{N_\Theta}(\bar{I}_o - \bar{I}_{b\Theta}) + (\bar{I}_{b\Theta} - \bar{I}_{b\Omega})\right| \leqslant \left|\frac{N_{\Theta_o}}{N_\Theta}(\bar{I}_o - \bar{I}_{b\Theta})\right| + |(\bar{I}_{b\Theta} - \bar{I}_{b\Omega})| \quad (2)$$

where $N_{\Theta_o}$ denotes pixels of object $\Theta$, $\bar{I}_o, \bar{I}_{b\Theta}$, and $\bar{I}_{b\Omega}$ are the average gray values of the object, the internal window, and external window, respectively. If the nature scene is a stable Gaussian noise, then $\bar{I}_{b\Theta} \approx \bar{I}_{b\Omega}$. $\Delta D$ reaches its extremum, when one of the following conditions holds.

$$\frac{N_{\Theta_o}}{N_\Theta}(\bar{I}_o - \bar{I}_{b\Theta}) = (\bar{b\Theta} - \bar{I}_{b\Omega}), \quad \Delta D = 2|\bar{I}_{b\Theta} - \bar{I}_{b\Omega}| \quad (3)$$

$$\frac{N_{\Theta_o}}{N_\Theta}(\bar{I}_o - \bar{I}_{b\Theta}) = 0, \quad \Delta D = |\bar{I}_{b\Theta} - \bar{I}_{b\Omega}| \quad (4)$$

$$\bar{I}_{b\Theta} - \bar{I}_{b\Omega} = 0, \quad \Delta D = \left|\frac{N_{\Theta_o}}{N_\Theta}(\bar{I}_o - \bar{I}_{b\Theta})\right| = \frac{N_{\Theta_o}}{N_\Theta}|\bar{I}_o - \bar{I}_{b\Omega}| \quad (5)$$

From (3), if $|\bar{I}_o - \bar{I}_{b\Theta}| \gg 0$ and $N_{\Theta_o} \ll N_\Theta$ for an object with concave contour, then $\Delta D$ is small. From (4), if $N_{\Theta_o} = 0$ or $\bar{I}_o = \bar{I}_{b\Theta}$ for no object, $\Delta D \approx 0$. In (5), when $N_{\Theta_o}$, $\Delta D \approx |\bar{I}_o - \bar{I}_{b\Omega}|$ and approaches to the maximum value.

It is obvious that for an erose object, 2-D AGADM-based method has two serious problems. First, when a target shape is abnormal such as rectangle and rotundity, the 2-D AGADM of the target is still low. Second, computing complexity is very huge. For every point, we need to calculate two dimensional average gray absolute difference for each internal window′s size in order to get its maximum value, so the complexity increases quadraticly with the size of the window.

### 2.2 Characteristic of the dissimilarity measure

Actually, most small targets are not of square. In order to solve the problem of low object dissimilarity measure, blur of object′s edge and the huge complexity, we split the two dimension windows in Fig. 1 into three one-dimensional interval in Fig. 2. The dissimilarity measure in Fig. 2 is just the same as that of the Fig. 1. Assuming the size of one dimensional external window is fixed, we can estimate the maximum average gray absolute difference for various sizes of the set $\Theta$. When $\Theta$ and $\Omega$ only cover object and background, respectively, the average gray absolute difference can get maximum value.

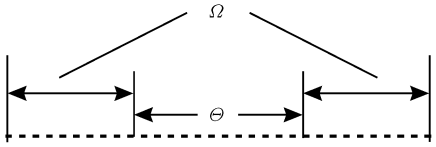


Fig. 2 1-D windows of object and scene

Because the dissimilarity is computed for each size of one dimensional windows, the size of one dimensional internal window can be changed to fit target region. So for abnormal target detection, one dimensional window has more flexibility than two dimensional windows. For convenience, a rectangle target is analyzed as shown in Fig. 3.

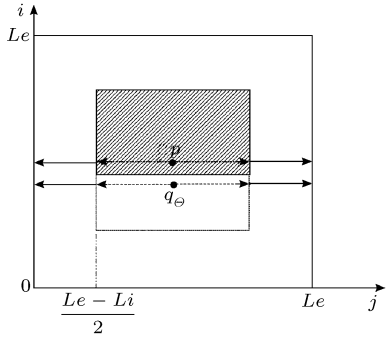


Fig. 3 The distribution of object and scene in inner and exterior windows

In Fig. 3, the inner and exterior windows are centered in point $p$, point $q$ is not the pixel of an object and the shadow window denotes object, broken line and real line windows are two dimensional internal window and external window, respectively. Broken arrow and real arrow denote 1-D internal window and external window centered in point $p$ and $q$, $Li$ and $Le$ are the sizes of internal window and external window, respectively. Assuming the regions of object and background are symmetrical, the average gray absolute difference can be computed as

$$\Delta D = \frac{R_{oi}\cdot\bar{G}_o + (R_i - R_{oi})\cdot\bar{G}_b}{R_i} - \frac{R_{oe}\cdot\bar{G}_o + (R_e - R_i - R_{oe})\cdot\bar{G}_b}{R_e - R_i} \tag{6}$$

where $R_{oi}$ and $R_{oe}$ denote the areas of object region between internal window and external window, respectively, $R_i$ and $R_e$ represent the area of 2-D internal window and external window, respectively, $\bar{G}_b$ and $\bar{G}_o$ ($\bar{G}_o > \bar{G}_b$) are the average gray values of object and the background, respectively. For point $p$ and $R_{oe} = 0$ the 2-D average gray absolute difference is

$$\Delta D_{P2} = \frac{R_{oi}}{R_i}(\bar{G}_o - \bar{G}_b) \tag{7}$$

while 1-D average gray absolute difference is computed as

$$\Delta D_{P1} = \bar{G}_o - \bar{G}_b \tag{8}$$

Comparing (7) and (8), we get $\Delta D_{P2} < \Delta D_{P1}$.

For point $q$, the two dimension average gray absolute difference is

$$\Delta D_{q2} = \frac{R_{oi}\cdot\bar{G}_o + (R_i - R_{oi})\cdot\bar{G}_b}{R_i} - \frac{R_{oe} + (R_e - R_i - R_{oe})\cdot\bar{G}_b}{R_e - R_i} \tag{9}$$

we have $0 < \Delta D_{q2} < \bar{G}_o - \bar{G}_b$ and 1-D average gray absolute difference is $\Delta D_{q1} = 0$.

For the 8 neighboring regions shown in Fig. 4, $Le$ denotes the size of 1-D and 2-D windows, the 2-D average gray absolute difference method has false edge in neighboring regions 2 and 6, but no false edge for 1-D average gray absolute difference method.

Because in object neighboring regions 1,3,5,7, $R_{oi} \neq R_i$ and $R_{oe} > 0$ from (6), the 2-D average gray absolute difference is greater than predefined threshold $T$, so the false edge appears while one 1-D average gray absolute difference equals 0, so no false edge. But in object neighboring regions 4, 8, both 1-D and 2-D average gray absolute differences are above predefined threshold T and both get false edge.

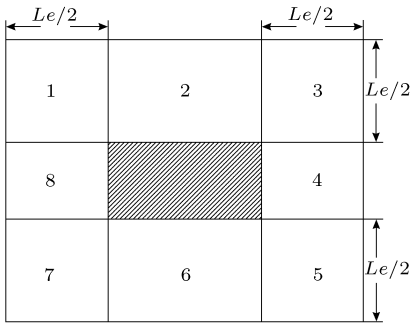


Fig. 4 The definition of 8-neighbour around object region

### 2.3 Algorithms of small object detection

One dimensional average gray absolute difference maximum algorithm (1-D AGADM)can be stated as follows.

**Step 1.** For any point of an image, given the fixed size $Le$ of an external window around the point, the maximum and the minimum average gray absolute differences are

$$\bar{G}\max = 0, \quad \bar{G}\min = 255$$

**Step 2.** If this point is the leftmost point of a row, let $Ge = 0$ and sum the gray values of all pixels in the external windows into $Ge$, otherwise, go to Step 3;

**Step 3.** Subtract the gray value of the leftmost point of the previous external window from $Ge$ of the previous point, then add the gray of the rightmost point of the current external window.

**Step 4.** Let the size of an internal window $Li = 3$, sum the gray values of all pixels in the internal window into $Gi$, let $\bar{G}i\max = 0$.

**Step 5.** $\Delta\bar{G} = \dfrac{Gi^*Le - Ge^*Li}{(Le - Li)Li}$, If $\Delta\bar{G} > \bar{G}i\max$, then $\bar{G}i\max = \bar{G}i$, else go to Step 6;

**Step 6.** $Li = Li + 2$, if $Li < Le - 2$, add the grays of the leftmost point and the rightmost point in the internal window into $Gi$, go to Step 5, else go to Step 7;

**Step 7.** Set the gray of current point in the 1-D AGADM $M$ to $\bar{G}i\max$;

**Step 8.** If $\bar{G}i\max > \bar{G}\max$, $\bar{G}\max = \bar{G}i\max$; if $\bar{G}i\max < \bar{G}\min$, $\bar{G}\min = \bar{G}i\max$;

**Step 9.** All points of the image have been processed completely? If no, go to Step 2;

**Step 10.** Normalize $\bar{G}$ and $\bar{G}$ into 255 and 0, respectively;

**Step 11.** Return.

## 3 Algorithm performance analysis

### 3.1 Computational complexity

To clarify the validity of the algorithm, the following paragraphs will discuss the comparison of computational complexity, signal-to-noise gain, and ROC curve of 1-D AGADM-based algorithm with that of 2-D ADADM-based algorithm[5], median contrast filter[6], and multi-level filter algorithm[7]. Assume that the image is an $r^*c$ matrix, and the size of the outside window is $Le$. When the outside window is shifted pixel by pixel, the gray sum of the last outside window can be utilized to estimate that of the current outside window by only adding or subtracting a pixel value. 1-D AGADM-based algorithm needs the number of $r^*[Le + 2^*(c - 1)]$ additions for a outside window. Similarly, adding number for the inside window is $r^*c^*(Le - 2)$. As a result, 1-D AGADM algorithm needs number of additions of $r^*[(c+1)Le-2]$. For 2-D AGADM algorithm, there are additions of $r^*Le^*[Le+2*(c-1)]$ and $r^*c^*(Le-2)^2$ for the outside window and inside window, respectively. Moreover, their numbers of multiplication are the same, having a value of $r^*c^*4$.

Define computation complexity, $C$, for each pixel as operations of the whole image (including additions and multiplications) divided by the number of the whole image′s pixels. In Fig. 5, the relationship between the computational complexity for 1-D AGADM and 2-D AGADM as a function of $Le$ is curved. It can be observed that when the size of the outside window is increased, complexity of the

2-D AGADM increases rapidly while 1-D AGADM just changes slightly and thus has great advantage in complexity.

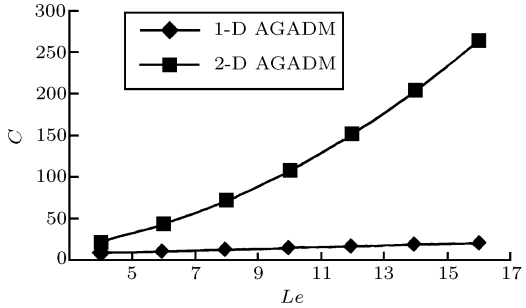


Fig. 5 Computational complexity per pixel of 1-D AGADM and 2-D AGADM

Table 1 The performance comparison of four algorithms of small object detection (original image size 200×196, SNR 0.31)

| | 1D AGADM | 2D AGADM | Median | Multi-level |
|---|---|---|---|---|
| Computation time (ms) | 1452 | 4356 | 2053 | 1252 |
| Shape adaptability | good | better | common | bad |
| SNR | 3.83 | 4.26 | 0.63 | 0.28 |

### 3.2 Signal-to-noise ratio gain

It has been known that the performance of detection algorithms is highly dependent on the signal-to-noise ratio of images, so we can use the ratio $Gs$ of the original image to the processed image as a performance measurement, which can be estimated as

$$Gs = \frac{SNR_r}{SNR_o} \tag{10}$$

where $SNR_o$ and $SNR_r$ are the signal-to-noise ratio of the original image and the processed image, and can be defined as follows.

$$SNR = \frac{|m_o - m_b|}{\sqrt{\sigma_b^2 + \sigma_o^2}} \tag{11}$$

where $m_b$, $m_o$, $\sigma_o$ and $\sigma_b$ stand for mean of an object, its background, deviation of object region, and background region, respectively.

Four object detection algorithms mentioned above have been tested with 10 different images of long-wave infrared offshore small-object and their changed versions by adding noise with different means and deviations. Fig. 6 represents the signal-to-noise ratio gains of those algorithms as a function of the input image signal to noise ratio for the fixed size object.

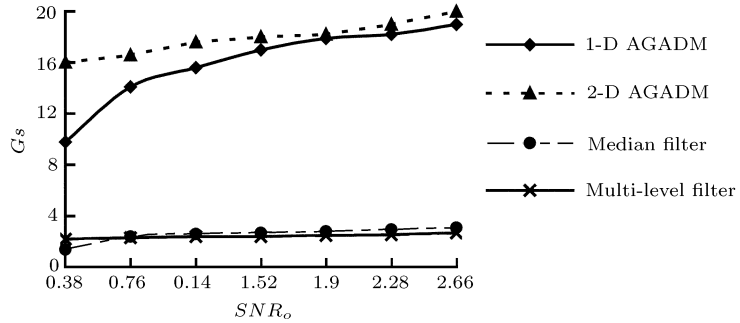


Fig. 6 Relationship between SNR gain and SNR of original images

### 3.3 Analysis of experimental results

Figs. 7 (a)∼(i) give a typical 200×196 image of long-wave infrared offshore small-object, and its filtered and segmented results. From Fig. 7, we know both median filtering and multi-level filtering algorithms have higher false alarm probability and 2-D AGADM can reduce noise greatly while enhancing object but with a rough contour. It has been shown from experimental results that 1-D AGADM algorithm can reduce noise and enhance object with an exact contour, and have lower complexity and shape adaptability.

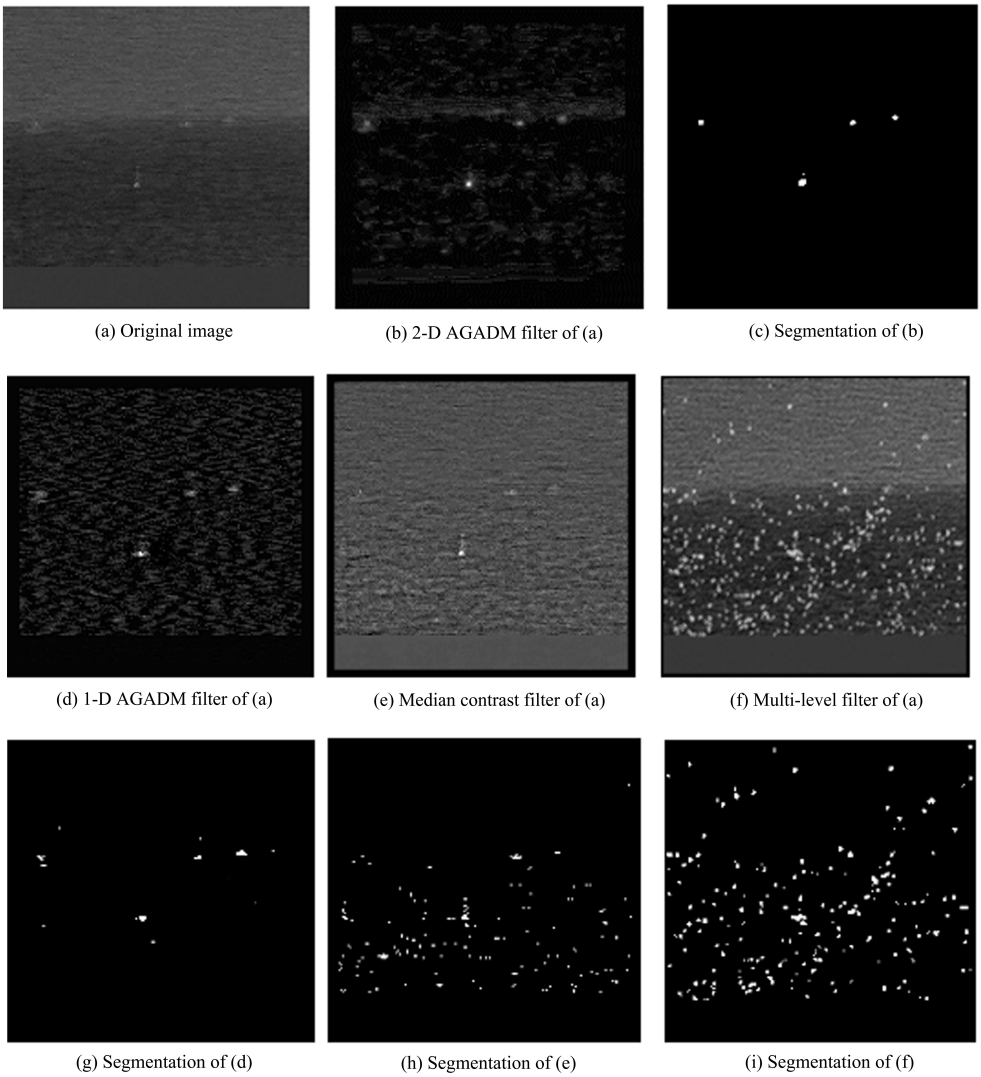


Fig. 7 Original image and its results of object detection

### 3.4 Receiver operating characteristic

For constant false alarm probability criterion, we can estimate the detection thresholds at various false alarm probability Pf, compute the detection probability Pd statistically, then depict a detection probability curve as a function of false alarm probability, which is called ROC curve. Four small target detection algorithms have been tested with 10 long wave infrared images of small targets and their ROC are computed and shown in Fig. 8.

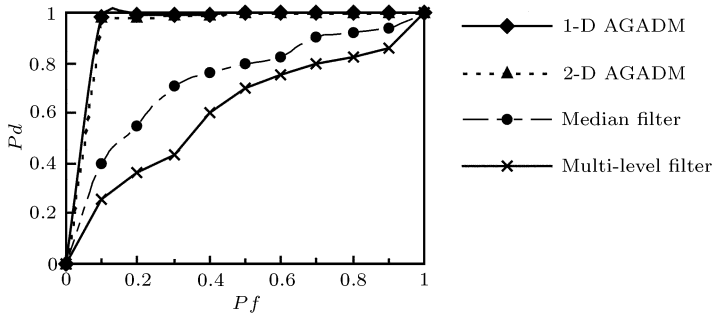


Fig. 8 The ROC curves of object detection algorithms

## 4 Conclusion

It has been shown that with an exception of slightly low SNR, this proposed algorithm has advantages of speed, shape adaptability over 2-D AGADM, and a greater SNR than the median filter and the multi-level filter algorithm, and can detect small targets with irregular shapes in a stable object/background image correctly. Finally, we can also use a smooth filter to reduce isolated noises and use shape features for false target identification.

## References

1 Wang J Y, Chen F S. 3-D object recognition and shape estimation from image contours using B-splines, shape invariant matching and neural network. *IEEE Transactions on Pattern Analysis and Machine Intelligence*, 1994, **16**(1): 13∼23

2 Mulassano P, Lo Presti L. Object detection on the sea surface, based on texture analysis. In: Proceedings of ICECS′99. The 6th IEEE International Conference on Electronics, Circuits and Systems, 1999. **2**: 855∼858

3 Shashua A. Projective structure from uncalibrated images: structure from motion and recognition. *IEEE Transactions on Pattern Analysis and Machine Intelligence*, 1994, **16**(8): 778∼790

4 Pell T. Multiscale fractal theory and object characterization. *Journal of the Optical Society of America A*, 1990, **7**(6): 1401∼1412

5 Wang Guo-You, Zhang Tian-Xu, Wei Luo-Gang, Sang Nong. Efficient method for multiscale small target detection from a natural scene. *Optical Engineering*, 1996, **35**(3): 761∼768

6 Sang Nong, Zhang Tian-Xu, Shi Wei-Qiang. Statistical analysis of contrast between infrared ship targets and background on sea-surface. *Infrared and Laser Engineering*, 1998, **27**(3): 9∼12

7 Cao Zhi-Guo, Zuo Zheng-Rong, Sang Nong, Zhang Tian-Xu. Parallel implementation for detecting small targets on infrared sea surface. *Journal of Huazhong University of Science and Technology*, 2001, **29**(12): 52∼54

**ZOU Yu-Lan** Received her bachelor and master degrees from Huazhong University of Science and Technology in 1997 and 2004, respectively. She currently is working in the Institute of Pattern Recognition and Artificial Intelligence at Huazhong University of Science and Technology. Her research interests include image modeling, computer vision, target detection, and intelligent approaches to image compression.

**WANG Guo-You** Received his bachelor and master degrees from Huazhong University of Science and Technology in 1988 and 1992, respectively. He is currently a professor in the Institute of Pattern Recognition and Artificial Intelligence at Huazhong University of Science and Technology. His research interests include image modeling, computer vision, fractals, target detection, and intelligent approaches to image compression.

**ZHANG Lei** Received his bachelor degree in automation control in 2003. Now he is a master student in the Institute at Pattern Recognition and Artificial Intelligence of Huazhong University of Science and Technology. His research interests include image modeling and target detection.